HHS Public Access

Author manuscript

Cell Calcium. Author manuscript; available in PMC 2017 April 01.

Published in final edited form as:

Cell Calcium. 2016 April ; 59(4): 145–155. doi:10.1016/j.ceca.2016.01.001.

Axial stretch-dependent cation entry in dystrophic cardiomyopathy: Involvement of several TRPs channels

E. Aguettaz[#a], **J.J. Lopez**[#b], **A. Krzesiak**[a], **L. Lipskaia**[c,d], **S. Adnot**[c], **R.J. Hajjar**[d], **C. Cognard**[a], **B. Constantin**[#b], and **S. Sebille**[#a,*]

[a] Laboratoire de Signalisation et Transports Ioniques Membranaires (STIM CNRS ERL 7368), Equipe Transferts Ioniques et Rythmicité Cardiaque (TIRC), Université de Poitiers, 86073 Poitiers Cedex 9, France

[b] Laboratoire de Signalisation et Transports Ioniques Membranaires (STIM CNRS ERL 7368), Equipe Calcium et Microenvironnement des Cellules Souches (CMCS), Université de Poitiers, 86073 Poitiers Cedex 9, France

[c] INSERM U955 and Département de Physiologie, Hôpital Henri Mondor, AP-HP, Université Paris-Est Créteil (UPEC), 94010 Créteil, France

[d] Cardiovascular Research Center, Icahn School of Medicine at Mount Sinai, New York, NY 10029, USA

[#] These authors contributed equally to this work.

Abstract

In Duchenne muscular dystrophy (DMD), deficiency of the cytoskeletal protein dystrophin leads to well-described defects in skeletal muscle but also to dilated cardiomyopathy (DCM). In cardiac cells, the subsarcolemmal localization of dystrophin is thought to protect the membrane from mechanical stress. The dystrophin deficiency leads to membrane instability and a high stress-induced Ca^{2+} influx due to dysregulation of sarcolemmal channels such as stretch-activated channels (SACs). In this work divalent cation entry has been explored in isolated ventricular Wild Type (WT) and *mdx* cardiomyocytes in two different conditions: at rest and during the application of an axial stretch. At rest, our results suggest that activation of TRPV2 channels participates to a constitutive basal cation entry in *mdx* cardiomyocytes.Using microcarbon fibres technique, an axial stretchwas applied to mimic effects of physiological conditions of ventricular filling and study on cation influx bythe Mn^{2+}-quenching techniquedemonstrated a high stretch-dependentcationic influx in dystrophic cells, partially due to SACs. Involvement of TRPs channels in this excessive Ca^{2+} influx has been investigated using specific modulators and demonstratedboth sarcolemmal localization and an abnormal activity of TRPV2 channels.

[*] Corresponding author at: ERL 7368 CNRS/Université de Poitiers, Pôle Biologie Santé Bât B36, 1 rue Georges Bonnet TSA 51106, 86073 Poitiers Cedex 9, France. Tel.: +33 549 453 767; fax: +33 549 454 014. stephane.sebille@univ-poitiers.fr (S. Sebille)..

Conflict of interest statement

None declared.

Appendix A. Supplementary data

Supplementary data associated with this article can be found, in the online version, at http://dx.doi.org/10.1016/j.ceca.2016.01.001.

In conclusion, TRPV2 channels are demonstrated here to play a key role in cation influx and dysregulation in dystrophin deficient cardiomyocytes, enhanced in stretching conditions.

Keywords

Duchenne muscular dystrophy; Dilated cardiomyopathy; Mdx; Mechanosensitivity; Calcium; Stretch-activated channels; Membrane stretch; TRPV2; TRPCs

1. Introduction

The Duchenne muscular dystrophy (DMD) is a severe X-linked disease affecting 1 in 3500 male births. Initially, DMD patients develop progressive weakness and loss the ability to walk around age 10. DMD is also associated by 20 years of age with cardiac complications including dilated cardiomyopathy (DCM) and arrhythmias, causing the death of about 20% of patients [1,2]. Mutations in the dystrophin gene on chromosome Xp21 result in the absence of the 427 kDa cytoskeletal protein dystrophin [3]. In cardiomyocytes, its subsarcolemmal and sarcomeric localization along the T-tubule network may be essential to maintain membrane integrity [4]. This protein is also a key component of the transmembrane dystrophin-associated glycoproteins (DAG) that connects cytoskeleton to the extracellular matrix [5]. It is thought that lack of dystrophin leads to mechanical instability of cell membrane [6] and renders it more susceptible to rupture [7], causing elevated Ca^{2+} influx and increased susceptibility to oxidative stress [8], which activate each other in a vicious cycle that contributes to DMD pathogenesis. Several studies have suggested that the rise in intracellular Ca^{2+} is an important initiating event in the pathogenesis of dystrophic muscle [9–11]. The increased Ca^{2+} entry occurring during activity, particularly during eccentric exercise, may lead to local proteolytic activation of cationic channels and results in a further increase of Ca^{2+} entry [12].

Stretch-activated channels (SACs) are thought to support excessive Ca^{2+} influx observed in dystrophic muscles [13]. SACs are a subcategory of mechanosensitive channels, which can switch from “closed” to “open” state in response to stretch alone or to a direct mechanical membrane deformation (see for review: [14]). They are permeable to Na^+, Ca^{2+} and K^+, and have been suggested to be primarily involved in the pathogenesis of DMD [15,16,17]. Cardiac SACs can be either cation non-selective (SAC_{ns}) or potassium-selective (SAC_k). SAC_{ns} are thought to be localized in membrane regions that are difficult to access for patch-clamp studies, such as T-tubules [18], caveolae [19], or intercalated discs [20]. Despite the lack of molecular identification, there are several prominent candidates for mammalian cardiac SACs. Genetic screenings in Saccharomyces cerevisiae, Caenorhabditis elegans, Drosophilia and *Danio rerio* indicated that transient receptor potential (TRP) channels subunits are involved in mechanical sensing [21–23]. TRP channels form a large family of cationic channels that likely function as tetramers in various processes and have been recently recognized as key molecules in pathological cardiac hypertrophy and heart failure [24,25].

Canonical TRP channels (TRPCs) are a group of mammalian Ca^{2+}-permeable channels which mediate store-operated Ca^{2+} entry as well as store-independent Ca^{2+} influx [26–28].

TRPC1 channels are widely expressed in cardiac myocytes and may be located in T-tubules [18] which are consistent with the hypothesized spatial distribution of endogenous SAC_{ns} [18]. In dystrophic fibres, TRPC1 have been involved in abnormal Ca^{2+} influx [29] and Ward et al. [30] have shown that expression level of TRPC1 was increased in aged *mdx*-DCM heart. TRPC1 was also shown to support elevated store-operated calcium entry in dystrophin deficient myotubes and fibres [29,31] as well as Orai1 in FDB fibres [32]. Studies in heterologous system demonstrated that TRPC1 expression induced a 10-fold increase of SAC_{ns} currents and TRPC1 inhibition through RNA anti-sens reduced these currents [33]. Subsequently, it has been shown that the specific SAC_{ns} blocker, GsMTx-4, blocked the expressed channel [34]. However, it has also been shown that GsMTx-4 could inhibit SACs formed probably with TRPC6 in smooth muscle [35]. TRPC6 is highly expressed in human heart homogenates [36]. This channel seems also to be located in T-tubules and can be translocated to the plasma membrane after stimulation with α_1-agonists [37]. Furthermore TRPC6 channels have been thought to be potential SAC_{ns} in ventricular cells as the related current could be blocked by a TRPC6 antibody [38]. Thus both TRPC1 and TRPC6 are good candidates for mammalian SAC_{ns}.

TPRV2 channels have also been involved in the stretch-dependent responses in different cell types as murine aortic myocytes or cardiomyocytes [39–41]. In a physiological context, these channels have been shown to be involved in the formation and integrity maintenance of intercalated discs and in the mechanotransduction in these particular areas [20]. Moreover, Rubinstein et al. [42] have demonstrated that TRPV2 channels could be involved in the molecular mechanisms of increased cardiomyocyte contractility. Indeed, authors have suggested that these channels may be involved in the sarcoplasmic reticulum (SR) Ca^{2+} load by a small local influx of Ca^{2+} in the vicinity of RyRs. Taking these results into account, TRPV2 seems to be also a good candidate for SAC_{ns}. In a pathological context, they have been demonstrated to be involved in the pathogenesis of myocyte degeneration in dystrophic muscle [43] and to support elevated divalent cation entry in human DMD myotubes [44]. Their sarcolemmal accumulation has been shown in dystrophic ventricular cardiomyocytes in several studies [40,41] suggesting a role in Ca^{2+} dysregulation that can lead to cardiomyocytes death.

Studying SACs is not trivial because of the need of technical skills and experience. Several methods have been developed to perform a mechanical stimulation including the use of glass microneedles [45], suction micropipettes [46] or adhesives [47]. Furthermore, others studies used cell swelling through hypoosmotic shock to investigate SACs activities in dystrophin deficient cardiomyocytes [41,48]. This latter technique leads to cell swelling through water entry, which is necessary for the balancing of ionic gradients between the extracellular medium and cytosolic compartment. The consequent increase of cell volume can provide a three-dimensional stretch of the cell, but changes in volume are not easily related to changes in tension. In the literature, authors agree that it is difficult to distinguish between the effects of the stretch component and other possible effects of swelling, i.e. changes in ions permeability can't be compared with those due to homogenous or local stretch [49].

In this work, divalent cation entry has been explored in isolated ventricular Wild Type (WT) and *mdx* cardiomyocytes in two different conditions: at rest and during the application of an

axial stretch. Ventricular cardiomyocytes have been stretched using a carbon microfibers technique [50,51], which has the advantage to achieve an almost homogenous lengthening of the sarcomeres and to best mimic the effect of diastolic filling in physiological conditions [52]. Moreover, the involvement of other channels, as store-operated channels, in the observed Ca^{2+} influx has been investigated with the use of channels blockers.

2. Materials and methods

2.1. Cells isolation

The investigation was conducted in agreement with European Community Council directives as well as with the Guide for the Care and Use of Laboratory Animals published by the US National Institutes of Health (NIH Publication No. 85-23, revised 1996).

Ventricular cardiac myocytes were isolated from 10 to 12 months male C57BL10Scsn (WT) mice and C57/BL10ScScn-*mdx* mice (Jackson Laboratory). Mice were euthanized by cervical dislocation, followed by rapid removal of the heart and subsequent enzymatic dissociation of the left ventricular tissue as previously described [53].

2.2. Solutions and chemicals

Before experiments, cells were stored in culture medium containing Dulbecco's modified Eagle's medium (DMEM—Lonza), complemented with 10 μg/mL insulin, 10 μg/mL gentamycin, 4 mM $NaHCO_3$, 10 mM Hepes, 0.2% BSA and 12.5 μM blebbistatin (all from Sigma). During experiments, cardiomyocytes were super-fused with Tyrode solution containing 140 mM NaCl, 5.4 mM KCl, 1.8 mM $CaCl_2$, 1.8 mM $MgCl_2$, 10 mM Hepes and 11 mM glucose or with calcium-free Tyrode solution containing 140 mM NaCl, 5.4 mM KCl, 1.8 mM $MgCl_2$, 10 mM Hepes, 11 mM glucose, 1 g/L BSA and 20 mM Taurine.

Tranilast (Trn) and TPEN (*N,N,N′,N′*-tetrakis-(2-pyridylmethyl)-ethylenediamine) was purchased from Calbiochem, THC (Δ9-tetrahydrocannabinol) from RTI International, the tarentula toxin GsMTx-4 from Abcam, Streptomycin sulfate (Strp) and 4-methyl-4′-[3.5-bis(trifluoromethyl)-1*H*-pyrazol-1-yl]-1.2.3-thiadiazole-5-carboxanilide (YM-58483) from Sigma, ryanodine from Merck, fura-2-AM and fluo-8-AM from Santa-Cruz.

2.3. Mechanical stimulation

Axial stretch of single myocyte was performed with the micro-carbon fibres technique previously described [51,52]. Briefly, a pair of carbon fibres (40 μm diameter, GRC—Graphite-reinforced carbon–TMIL—Tsukuba Materials Information Laboratory, Ltd, Tsukuba, Japan) was mounted in glass capillaries, whose thin ends were bent by 30° to ensure near-planar approach to the cell surface. The end of each carbon fibre was attached to the ends of a cardiomyocyte (CF1 and CF2 in Fig. 2A), using two separate three-axis miniature hydraulic manipulators. Axial stretch was performed through the lateral movement of one fibre (CF2, bold black arrow in Fig. 2B) and sarcomere length was measured with a high-speed camera and dedicated software (Sarclength, Ionoptix) that uses a FFT procedure for the measurement. Axial stretch was applied during 30 s before Mn^{2+} perfusion and was maintained during the recording time, i.e. around 60 s.

2.4. Mn^{2+}-quenching experiments

Cardiomyocytes were incubated for 45 min at 37 °C, 5% CO_2 in culture medium with 3 μM (final concentration) of fura-2-AM probe. After being loaded, cells were washed with Ca^{2+}-free Tyrode solution before measurement of cation influx. Fura-2 loaded cells were excited at 360 nm with a CAIRN monochromator (Cairn Research Limited, Faversham, UK), and emission fluorescence was monitored at 510 nm using a CCD camera (Photonic Science, Robertsbridge, UK) coupled to an Olympus IX70 inverted microscope (60X water immersion fluorescence objective). The influx of Mn^{2+} through cationic channels was evaluated by the quenching of the fura-2 fluorescence excited at 360 nm, i.e., at the isosbestic point. The variation of fluorescence was recorded through the Imaging Workbench 4.0 (IW 4.0) software (Indec BioSystems, Mountain View, CA). The rate of fluorescence intensity loss at 510 nm was divided by the initial fluorescence intensity in the cell measured before the addition of manganese ions to correct for differences in the cell size or fura-2 loading. This computed value is indicated as F360 throughout all the paper. The maximal rate of quench of the fluorescence intensity, expressed as percent per minute, was obtained using a linear regression analysis.

2.5. Tissue preparation and confocal immunofluorescence

The hearts were fixed with 4% formalin (m/v) overnight and then were embedded in paraffin. Paraffin-embedded sections were deparaffinized using xylene and a graded series of ethanol dilutions then incubated in citrate buffer (0.01 M, pH 6) at 90 °C for 20 min for epitope retrieval. Sarcolemma or sarcomeric structure (F-actin) of cardiomyocytes were visualized using Wheat Germ Agglutinin FITC conjugate (WGA, W11261, Invitrogen) or Phalloidin FITC conjugate (P2141, Sigma-Aldrich) respectively. Immunolabelling with a-TRPV2 (ACC-039, Alomone lab) was performed using standard protocol including a permeabilization step with 0.1% Triton X-100 in PBS for 10 min. Secondary antibody was a-rabbit IgG conjugated with Alexa 555 (Invitrogen). Tissue sections were examined with a Zeiss LSM-510 confocal scanning laser microscope equipped with a 25 mW argon laser and a 1 mW helium-neon laser, using a Plan Apochromat 63× objective (NA 1.40, oil immersion). Green fluorescence was observed with a 505–550 nm band-pass emission filter under 488 nm laser illumination. Red fluorescence was observed with a 560 nm long-pass emission filter under 543 nm laser illumination. Pinholes were set at 1.0 Airy units. Stacks of images were collected every 0.7 μm along the *z*-axis. All settings were kept constant to allow comparisons. For double immunofluorescence, dual excitation using the multitrack mode (images taken sequentially) was achieved using the argon and He/Ne lasers. ImageJ software was used according to the guidelines to construct multi-channel images.

2.6. Immunoblot analysis

Protein samples were prepared using a lysis buffer containing protease and phosphatase inhibitors (Roche), separated by SDS-PAGE and transferred on nitrocellulose membranes (Millipore). The membranes were blotted using standard protocol and revealed by chemiluminescence (Pierce). The following antibodies were used: anti-TRPV2 (ACC-039, Alomon lab); anti-beta Actin (ab16039, Abcam). The densities of the immune-reactive bands were quantified using ImageJ software (NIH).

2.7. Statistical analysis

Data are presented as means ± SEM, n is the number of cells. Differences were tested with *t*-test. $P < 0.05$ indicates a statistical significant difference.

3. Results

3.1. Cation influx in resting conditions

Basal cation entry in isolated cardiomyocytes was recorded using the quenching of fura-2 fluorescence by manganese. With this technique, Mn^{2+} ions are assumed to enter the cell through the same pathways as the ones used by Ca^{2+}, and once within the cells, these ions are trapped in the cytosol and strongly quench the fluorescence emitted by the fura-2 Ca^{2+} dye. The perfusion of Mn^{2+} solution generated no or weak (1.40 ± 2.36%/min $n = 19$) basal cation entry in cardiomyocytes from WT mice (Fig. 1A). On the contrary, perfusion of Mn^{2+} solution on *mdx* non-stimulated (rest) cardiomyocytes led to a significant cation entry (10.34 ± 5.07%/min $n = 12$). This entry was observed only in dystrophin-deficient cardiomyocytes and suggested that sarcolemmal cation channels were constitutively active during the recording. Previous experimental data have shown that *mdx* skeletal muscle fibres exhibited increased permeability to divalent cations that enter the cell through channel-blocker sensitive pathways [54]. In our experiments, since divalent cation influx are also altered in *mdx* cardiomyocytes, a panel of cation and calcium channels inhibitors or agonists was introduced during the Mn^{2+} solution perfusion (Fig. 1B).

TRPV2 has been shown to constitute a major input path of Ca^{2+} in dystrophic striated muscle [41,44,55]. Given the essential implication of TRPV2 shown in *mdx* and the protective effect of its down-regulation, we considered studying the dependency of divalent cation influx on TRPV2. We first used Δ9-tetrahydrocannabinol (THC), a well-known activator of human and rat TRPV2, [56]. Divalent cation entry was recorded in WT and mdx cardiomyocytes after the introduction in the extracellular medium of Mn^{2+} solution supplemented with 10 μM THC. Perfusion with THC activated a significant divalent cation influx in WT cardiomyocytes (Fig. 1B), suggesting that TRPV2 channels can be activated in isolated normal cardiomyocytes. Nevertheless, the level of THC-induced divalent cation influx observed in WT cells was found lower than the level of constitutive divalent cation entry recorded in *mdx* cardiomyocytes. THC stimulation did not activate a significant supplemental divalent cation entry in *mdx* cells that already exhibited basal cation influx (Fig. 1B). Although the TRPV2 agonist THC was not able to increase divalent cation entry, the two TRPV2 inhibitors tranilast (Trn, 100 μM) and ruthenium red (RR, 1 μM) led to a reduction of more than 50% of the constitutive influx in mdx cardiomyocytes. This suggest that a constitutive activation of TRPV2 channels participated to the basal divalent cation entry, but that THC is not able to increase this basal activation in mdx cardiomyocytes.

The early work of Hopf and collaborators [57], suggested that the over-activated “leak channels” recorded in *mdx* and DMD skeletal muscle cells could be store-operated cationic channels. Other studies confirmed the overactivation of store-operated channels (SOCs) in *mdx* skeletal muscle cells [29,58]. This led us to test if basal divalent cation entry in cardiomyocytes could be partly supported by SOCs. YM-58483, characterized as a selective

inhibitor of store-operated calcium entry [59,60] was applied on *mdx* cardiomyocytes during perfusion of Mn^{2+} solution. This incubation led to a drastic decrease of divalent cation influx at rest, suggesting that both TRPV2 and SOCs may participate to the basal cation entry observed in dystrophic cardiomyocytes. This was confirmed by a more severe reduction of divalent cation influx after treatment with the two blockers YM-58483 and RR.

Incubation with 10 μM of the voltage-gated channel inhibitor nifedipine, known to selectively inhibit voltage-dependent L-type calcium channels at this concentration, did not affect cation influx recorded in mdx cardiomyocytes (Fig. 1B). This result allowed ruling out the participation of voltage-gated channels in the recorded influx.

We also investigated if, in our model, a calcium influx could be triggered by SR depletion, thus, SR calcium stores were depleted with the use of *N,N,N′,N′*-tetrakis(2-pyridylmethyl)ethilenediamine (TPEN) which is able to chelate SR calcium stores. Once SR stores were depleted, Mn^{2+} solution was introduced into the extracellular medium and cation influx was recorded (Fig. 1C). A store-dependent cation entry could be recorded in WT cardiomyocytes after treatment with the SR Ca^{2+} chelator. This influx was almost two fold higher in mdx cardiomyocytes as compared to normal ones but was not significantly different from basal divalent cation entry measured without treatment in the same cell type. This suggests that channels supporting the basal divalent cation entry are the same channels that are mobilized after TPEN treatment. This may illustrate a cooperative activation of TRPV2 channels and SOCs in the sarcolemma of mdx myotubes when the dystrophin-associated protein complex is disrupted.

3.2. Cation influx in axial stretch conditions

Ventricular cardiomyocytes were stretched using the carbon microfibers technique (Fig. 2) described in the materials and methods part. In all experiments, sarcomere length was controlled through the use of a high-speed camera and a dedicated software (Sarclength, Ionoptix). Before stretch, sarcomere length has been computed for each cardiomyocyte and was found equal to 1.81 ± 0.01 μm for WT (n = 130) and 1.78 ± 0.01 μm for *mdx* (n = 130). Axial stretch was carried out through lateral movement of the CF2 fibre (Fig. 2A and B) and the amount of stretch was graded to cause a 10% increase of sarcomere length, corresponding to a 0.18 μm increase.

Fig. 2C illustrates the quenching of fura-2 fluorescence in axial-stretched cardiomyocytes or at rest in response to Mn^{2+} perfusion. Maintaining WT cardiomyocytes in stretch conditions generated an important decrease of the fura-2 fluorescence. In *mdx* cardiomyocytes, the decrease observed after the perfusion of Mn^{2+} in resting conditions was further enhanced in stretched *mdx* and found to be higher than in stretched WT cardiomyocytes. These results demonstrate that axial stretch allows significant sarcolemmal influx in WT and *mdx* cardiomyocytes.

3.3. Involvement of SACs in stretch-dependent cations influx

In order to investigate which channels are involved in cation entry observed in our experiments, particularly in stretch conditions, inhibitors of SACs and L-type Ca^{2+} channels have been used. Bars in Fig. 2D represent cation entry at rest and during axial stretch in both

WT and mdx cardiomyocytes measured as the mean slope of fura-2 fluorescence intensity decrease (in %/min). Stretch conditions showed higher cation entries as compared to resting conditions in both WT (25 ± 3%/min n = 14, white bars and 1.4 ± 0.5%/min n = 19, clear grey declined hatching, respectively) and mdx cardiomyocytes (49 ± 7%/min n = 14, white bars *and* 10.3 ± 1.5%/min n = 12, clear grey declined hatching, respectively). Regarding stretch, first, in control conditions (white bars) stretched *mdx* cardiomyocytes showed a higher cation entry as compared to stretched WT (49 ± 7%/min n = 14 and 25 ± 3%/min n = 14, respectively). Second, cardiomyocytes were incubated in the presence of SACs blockers to assess their involvement in the stretch-dependent cation influx. The aminoglycoside antibiotic streptomycin (Strp) has been reported to be a non-specific inhibitor for SACs and to reduce Ca^{2+} leak influx in resting muscle [30]. In WT cardiomyocytes, incubation with 300 μM Strp strongly inhibited stretch-dependent cation influx to 1.6 ± 0.7%/min n = 13 (grey bar) whereas in *mdx* cardiomyocytes, incubation with Strp only partly blocked this influx to 10 ± 3%/min (n = 12). The most specific inhibitor for SACs available today is the tarantula spider toxin GsMTx-4 [61,62]. Likewise, in WT cardiomyocytes, incubation with 2.5 μM GsMtx-4 (black bars) reduced the fluorescence quenching rate to 6 ± 1%/min (n = 5) whereas in *mdx* cardiomyocytes, GsMTx-4 incubation reduced stretch-dependent cation influx to 26 ± 1%/min (n = 4). In addition, the possible involvement of L-type Ca^{2+} channels has also been studied using nifedipine. In WT cardiomyocytes, incubation with 10 μM nifedipine (vertical hatching) failed to lead to any inhibition of cation influx (to 38 ± 3%/min n = 5) and led only to a weak reduction in *mdx* cardiomyocytes (24 ± 6%/min n = 6). Taken together, these results suggest that stretch-dependent cation influx could be more partly due to SACs rather than L-type Ca^{2+} channels.

These results indicate first that stretch-dependent cation influx are strongly inhibited by SACs blockers in WT cardiomyocytes, meaning that axial stretch could induce SACs activation in normal conditions. Second, activation of SACs was also observed in the pathological condition of dystrophin-deficiency (*mdx*-DCM model) and this activation was found to be higher than in WT. Finally, the divalent cation entry in response to axial stretch was found higher than the constitutive cation influx observed in mdx cardiomyocytes in resting conditions.

3.4. Involvement of TRPV2 channels in stretch-dependent cation influx

Because TRPV2 channels have been identified as molecular candidates for stretch-activated channels [39,63] their involvement were investigated in our *mdx*-DCM model (Fig. 3). Fig. 3A illustrates the quenching of fura-2 fluorescence in stretched cardiomyocytes in response to Mn^{2+} perfusion in the presence of an antibody raised against an extracellular epitope of the channel (AB TRPV2 extra), that could potentially block TRPV2 channels. In WT cardiomyocytes (filled triangles), incubation with AB TRPV2 extra (open triangles) did not modify fura-2 fluorescence intensity decrease during per-fusion of Mn^{2+} whereas in *mdx* cardiomyocytes (filled circles), AB TRPV2 extra incubation (open circles) led to a strong inhibition.

Fig. 3B displays stretch-dependent cation influx in the presence of AB TRPV2, Tranilast (Trn), and YM-58483 (YM). Effects have been calculated as maximal slopes of the Mn^{2+}-

induced decreasing phase of fura-2 fluorescence (F_{360}) and expressed as percent decrease per minute. In WT cardiomyocytes, incubation with AB TRPV2 extra failed to block the cation influx (28 ± 7%/min n = 5 dark grey bars) observed in control (25 ± 3%/min n = 14 white bars) whereas in *mdx* cardiomyocytes, a strong inhibition could be observed (to 7 ± 2%/min n = 6, dark grey bar) in the presence of this antibody, as compared to control (49 ± 7%/min n = 14, white bar). Similar effects could be observed with Tranilast (Trn), for which it has been reported a strong specificity for TRPV2 channels. In WT cells, incubation with 100 μM Trn did not significantly reduce the cation influx (19 ± 4%/min (n = 13) light grey bar) as compared to control (25 ± 3%/min n = 14, white bar). In *mdx* cardiomyocytes, Trn incubation drastically reduced the cation influx (9 ± 2%/min n = 13, light grey bar) as compared to control (49 ± 7%/min n = 14). The application of 2 μM of YM-58483, induced a high inhibition of the cation influx both in WT and mdx cardiomyocytes (5 ± 2%/min n = 10 horizontal hatching, and 9 ± 3%/min n = 7 horizontal hatching, respectively). Moreover, in *mdx* cardiomyocytes, incubation with 100 μM Trn and 2 μM YM almost completely blocked cation influx (data not shown).

3.5. TRPV2 channels expression in WT and mdx cardiomyocytes

Taking into account the preceding results, immunostaining of TRPV2 channels has been performed with anti-TRPV2 antibody (Fig. 4) and a difference of TRPV2 localization was observed between WT (Fig. 4A) and *mdx* (Fig. 4B). In WT cardiomyocytes, TRPV2 immunostaining revealed sarcolemmal and intracellular localizations of this protein. By contrast *mdx* cardiomyocytes displayed only a significant TRPV2 localization at the sarcolemma. Fluorescence profiles drawn at the yellow line position show the sarcolemmal enrichment of TRPV2 *mdx* cardiomyocytes (Fig. 4D) as compared to WT (Fig. 4C). In order to evaluate sarcolemmal TRPV2 immunostaining, quantification of fluorescence intensity at the periphery of the cell, relative to intracellular fluorescence intensity, has been performed (Fig. 4E and F). Hence, from immunostaining images profiles, it was possible to determine the sarcolemmal fluorescence intensities S1 and S2 (Fig. 4E) and the mean (S) of these two values was divided by the minimal fluorescence intensity value in the profile (C: Fig. 4E). The determined ratio S/C (Fig. 4F) was obtained in images from WT (n = 11 cells) and *mdx* (n = 13 cells) cardiomyocytes. A significant difference was found between this ratio in mdx as compared to WT, suggesting a relative higher sarcolemmal localization of TRPV2 in *mdx* cardiomyocytes.

Fig. 4G shows an example of western blot obtained from isolated left ventricular WT and *mdx* cardiomyocytes, and TRPV2 expression is shown relative to actin expression. No drastic difference was found in the whole expression levels of TRPV2 in WT and *mdx*. Nevertheless, a two bands profile was observed with a marked presence of a light band in *mdx*. This profile could be related to the presence of two different TRPV2 forms. Distribution of the two bands has been analysed (Fig. 4H). The ratio of band densities (a band/b band) showed a different distribution between WT and *mdx*. Indeed, band a was more represented in WT cardiomyocytes (a/b = 1.44 ± 0.07 (n = 4)). In *mdx* cardiomyocytes, band b was found equivalent to band a (0.95 ± 0.13 (n = 4)), bringing to mind the possibility of a small TRPV2 variant expression increased in dystrophin-deficient context.

Because intracellular localization of TRPV2 channels may be affected in in vitro conditions, we have performed immunolocalization of TRPV2 channels on cross sections of WT and *mdx* hearts (Fig. 5). Sarcolemma and sarcomeric structure (F-actin) were visualized using WGA or phalloidin staining, respectively (Fig. 5). As it is demonstrated on Fig. 5A, regions of robust sarcolemmal expression of TRPV2 can be observed on the cardiomyocytes from mdx mice, but not on the cardiomyocytes of WT mice. Fluorescence profiles drawn at the yellow line position confirm the sarcolemmal localizations of TRPV2 *mdx* cardiomyocytes (Fig. 5B). Co-immunostaining with phalloidin-FITC revealed that in WT cardiomyocytes TRPV2 are located mainly on the longitudinal sarcoplasmic reticulum network that wrap around the myofibrils (Fig. 5C), whereas in mdx cardiomyocytes TRPV2 seems to be located both on the longitudinal sarcoplasmic reticulum network and on the sarcolemma or closely to sarcolemma (Fig. 5C). Noteworthy, in the mdx cardiomyocytes TRPV2 expression was higher on the sarcolemma than on the sarcoplasmic reticulum.

4. Discussion

Taken together, these findings suggest that activation of TRPV2 channels participates to a constitutive basal cation entry in *mdx* cardiomyocytes. Interestingly, channels supporting the basal divalent cation entry are the same channels that are mobilized after TPEN treatment. This may illustrate a cooperative activation of TRPV2 channels and SOCs in the sarcolemma of *mdx* myotubes when the dystrophin-associated protein complex is disrupted.

Moreover, using a carbon microfibers technique, an axial stretch was applied to mimic effects of physiological conditions of the ventricular filling and study on divalent cation influx by the Mn^{2+}-quenching technique demonstrated a high stretch-dependent cation influx in dystrophic cells, partially due to SACs. The stretch-dependent Ca^{2+} influx was found to depend, in WT cardiomyocytes, on other channels than TRPV2. These channels could be TRPC that are blocked by YM-58483 (BTP2), and can be activated by stretch as it was suggested for TRPC1 and TRPC6 [33,35]. In *mdx* cardiomyocytes, the stretch-dependent Ca^{2+} entry depends both on TRPV2 and TRPCs channels, meaning that TRPV2 channels could play a key role in the calcium dysregulation in *mdx* cardiomyocytes, enhanced in stretching conditions.

4.1. Constitutive cation entry at rest in mdx cardiomyocytes

It was already suggested that divalent cation permeability was increased at rest in dystrophic mouse skeletal muscle fibres when measured by the Mn^{2+}-quenching technique [54]. Here we demonstrated the presence of a constitutive divalent cation entry in dystrophic mouse cardiomyocytes measured at rest by the same technique and absent in normal cardiomyocytes. The pharmacological characterization of this constitutive divalent cation entry suggested that both TRPV2 and SOC participate and may cooperate to this increased permeability. It was already proposed that a pool of TRPV2 at the sarcolemma could be constitutively active and that Ca^{2+} entry may promote the addressing of cytoplasmic TRPV2 in dystrophic cardiomyocytes [43]. Moreover, the constituents of SOCs, Orai and TRPC1 proteins, were shown to support elevated calcium influx after store depletion in dystrophic myotubes and fibres, when deficient in dystrophin [29,31,32]. Interestingly, TRPC1 was also

suggested to support a constitutive calcium entry in skeletal muscle fibres when deficient in homer-1 [64], and we showed that the scaffolding protein α1-syntrophin prevents exacerbated TRPC1-dependent cation entry in skeletal myotubes [31]. TRPC1 was also shown to be enriched at the sarcolemma of mdx fibres and associated with caveolin-3. This may maintain the channel at the membrane, where TRPC1 are deregulated because of the absence of α1-syntrophin [31]. Altogether, this suggests that the absence of the dystrophin/syntrophin/homer-1 scaffold, which is deficient in dystrophic muscles is responsible of TRPC1 and also TRPV2 deregulation at the sarcolemma. This may lead to a constitutive activity of TRPV2 and/or TRPC1, which participates to the observed diva-lent cation influx in *mdx* cardiomyocytes at rest. In their previous work, Iwata and collaborators [43] showed that the sarcolemmal translocation of TRPV2 was dependent on a calcium influx, and suggested that a pool of constitutively active TRPV2 channels could promote this translocation. Alternatively, both TRPC and TRPV2 constitutively active channels could promote the elevated calcium-dependent translocation of TRPV2 to the sarcolemma of dystrophic cardiomyocytes and in turn, exacerbate the calcium entry at rest or during stimulation.

4.2. Axial stretch-dependent influx and SACs

It is widely accepted that membrane of dystrophin-deficient cardiomyocytes is more fragile, making these cells more susceptible to mechanically induced damage. This loss of membrane integrity leads to an increase of permeability which allows an abnormal stress-induced influx of Ca^{2+}. The stretch-activated channels (SACs) have been proposed to mediate these abnormal Ca^{2+} entries in DMD skeletal muscle [15,65] and in *mdx* cardiomyocytes [41,48]. Nevertheless, in these studies, the mechanical stress applied on cardiomyocytes was a hypoosmotic shock which triggers a cell swelling. In this condition, are the same channels involved in a physiological diastolic stretch? In this study, an homogenous axial stretch was carried out to mimic the effects of a diastolic stretch.

The present results show that an homogenous axial stretch can create conditions for the presence and/or the activation of cationic permeant sarcolemmal channels. The cation influx observed in *mdx* cardiomyocytes is higher than influx observed in WT in agreement with the hypothesis of dysregulation of sarcolemmal calcium channels. This observed cation influx can been attributed, in part, to activation of stretch-activated channels (SACs). The evidence is based on the results obtained from a combination of two inhibitors: streptomycin, which is not only a blocker of SACs but can also modulate Ca^{2+} and K^{+} channels in cardiac muscle [66,67], and the most specific inhibitor of cationic non selective SACs known today, the tarentula toxin, GsMTX-4. These two SACs blockers lead to the diva-lent cation influx inhibition, although not completely. This later observation suggests that cation influx pathways other than SACs are present as well.

It has been demonstrated that axial stretch can induce depolarization of the resting potential and prolongation of the action potential which can trigger after-depolarization and extrasystoles [68]. These results would suggest an increase of Ca^{2+} influx through L-type Ca^{2+} channels. Here, the use of nifedipine did not significantly modify the stretch-dependent cation influx which excludes, in our conditions, the activation of these channels by axial

stretch and the consecutive calcium entry through this pathway. However, the entry of both Ca^{2+} and Na^{+} through TRPC channels could also participate to membrane after-depolarization following axial stretch.

4.3. TRPV2 channel: A likely SACs candidate in mdx cardiomyocytes

In the present study, a stretch-dependent influx, higher than in resting conditions, has been demonstrated and this sarcolemma influx seems to be mediated at least partly by SACs. The molecular identity of SACs involved in muscular dystrophy is unknown. However, some studies have proposed several candidates as potential SACs in *mdx* cardiomyocytes such as TRPV2 channels. Recently, a number of studies involved these channels in a pathological context of heart disease but are also focused on their physiological role. Indeed, TRPV2 channels seem to be involved in the formation and the maintenance of integrity of the intercalated disks and have a key role in the mechanotransduction in these specific areas of cardiomyocytes [20]. In DMD, TRPV2 channels have been suggested to be involved in the progression of the pathology in both skeletal and cardiac muscle with an abnormal sarcolemmal localization [40,41]. TRPV2 channels were also shown to be enriched at the sarcolemma of DMD human skeletal myotubes and to support an exagerated divalent cation entry in response to THC [44]. Here, a sarcolemmal accumulation has also been observed in aged *mdx* cardiomyocytes, and in WT the localization was found more intracellular. To assess the function of these channels in our model, different pharmacological tools have been used. First, inhibition of TRPV2 channels through application of a blocking antibody raised against an extracellular epitope of these channels (AB TRPV2 extra) strongly reduced the stretch-dependent cation influx in *mdx* but not in WT cardiomyocytes. This could be related to the sarcolemmal localization in *mdx* cells. Second, the use of an another, less specific, blocker of TRPV2 channels, tranilast, confirmed the data previously obtained with extracellular application of AB TRPV2 extra.

Moreover, the presence of a light band in *mdx* TRPV2 western blots seems to indicate the expression of two different proteins and make possible the presence of a TRPV2 variant expression. Indeed, it as already been demonstrated that osmosensensory transduction in mouse supraoptic nucleus neurons is depending on an N-terminal variant of TRPV1 channel and not on the full-length protein [69]. Moreover, a short splice variant of TRPV2 has already been detected in urothelial [70] and human leukemic cells [71]. The small TRPV2 variant identified in these studies was lacking on the pore forming region and sixth transmembranar domain. In our case, a naturally occuring alternative splice variant may interact with the full length TRPV2, or other TRP channels and could modify traffic-king, translocation to the plama membrane, and finally contribute to increased calcium influx in *mdx* cardiomyocytes.

4.4. SOCs channels: SACs candidates in WT cardiomyocytes?

It was found in this study that the YM-58483 blocker was able to reduce cation influx in axial-stretched WT and *mdx* cardiomyocytes. YM is known to inhibit SOCs channels as Orai1 and TRPCs channels [60]. Among these SOCs channels, TRPCs channels have already been described as potential SACs canditates [33,35]. Studies about TRPCs mechanosensitivity are controversial because of the lack of specific tools and most of the

studies have been performed in heterologous systems. Moreover, because a direct mechanosensitivity of these channels has not been clearly prooved, the recent idea is that the stretch sensitivity could be indirect and needed one or more others components [23]. Nevertheless, it has been demonstrated that TRPC1 expression level was increased in patholological context of DMD [30] and RNA antisens of TRPC1 channels in skeletal myoblasts can reduce SACs activity [29]. TRPC6 channels have also been identified as SACs in a study where I_{SAC} was inhibited by pore blocking antibodies [37]. In our experiments, the stretch-dependent cation influx seemed to be partly due to TRPCs channels because the use of the non-specific blocker of TRPCs channels, YM-58483, induced a strong inhibition in both WT and *mdx* cardiomyocytes.

in this study, aged dystrophin-deficient cardiomyocytes respond to a mechanical challenge differently from WT cells. Indeed, our results support the involvement of different type of channels involved in the stretch-dependent response with an abnormal cation influx which could induce by it's own an increase of the intracellular calcium concentration. TRPV2 channels are demonstrated here to play a key role in Ca^{2+} influx and dysregulation in stretched dystrophin deficient cardiomyocytes. Thus, the function and the translocation pathway of TRPV2 channels could be relevant targets for pharmacological therapy of DMD pathology.

Supplementary Material

Refer to Web version on PubMed Central for supplementary material.

Acknowledgments

This work was supported by grants (Nos. 16791 (EA, AK, CC, SS) and 16442 (JJL, LL, RJH, BC)), thesis fellowship (EA) and Postdoctoral fellowship (JJL) from the Association Française contre les Myopathies-Telethon and in part by NIH RO1 HL083156, HL080498, HL093183, and P20HL100396 (RJH).

We thanks the imaging Platform ImageUP for its technical assistance.

References

1. Ferlini A, Sewry C, Melis MA, Mateddu A, Muntoni F. X-linked dilated cardiomyopathy and the dystrophin gene. Neuromuscul. Disord. 1999; 9:339–346. [PubMed: 10407857]
2. Spurney CF. Cardiomyopathy of Duchenne muscular dystrophy: current understanding and future directions. Muscle Nerve. 2011; 44:8–19. [PubMed: 21674516]
3. Monaco AP, Bertelson CJ, Middlesworth W, Coletti CA, Aldridge J, Fischbeck, et al. Detection of deletions spanning the Duchenne muscular dystrophy locus using a tightly linked DNA segment. Nature. 1985; 316:842–845. [PubMed: 2993910]
4. Lorin C, Gueffier M, Bois P, Faivre JF, Cognard C, Sebille S. Ultrastructural and functional alterations of EC coupling elements in *mdx* cardiomyocytes: an analysis from membrane surface to depth. Cell Biochem. Biophys. 2013; 66:723–736. [PubMed: 23400933]
5. Sharpe KM, Premsukh MD, Townsend D. Alterations of dystrophin-associated glycoproteins in the heart lacking dystrophin or dystrophin and utrophin. J. Muscle Res. Cell Motil. 2013; 34:395–405. [PubMed: 24096570]
6. Gailly P. New aspects of calcium signaling in skeletal muscle cells: implications in Duchenne muscular dystrophy. Biochem. Biophys. Acta. 2002; 1600:38–44. [PubMed: 12445457]

7. Petrof BJ, Shrager JB, Stedman HH, Kelly AM, Sweeney HL. Dystrophin protects the sarcolemma from stresses developed during muscle contraction. Proc. Natl. Acad. Sci. U.S.A. 1993; 90:3710–3714. [PubMed: 8475120]
8. Lawler JM. Exacerbation of pathology by oxidative stress in respiratory and locomotor muscles with Duchenne muscular dystrophy. J. Physiol. 2011; 589:2161–2170. [PubMed: 21486793]
9. Whitehead NP, Streamer M, Lusambili LI, Sachs F, Allen DG. Streptomycin reduces stretch-induced membrane permeability in muscles from *mdx* mice. Neuromuscul. Disord. 2006; 16:845–854. [PubMed: 17005404]
10. Hopf FW, Turner PR, Steinhard RA. Calcium misregulation and the pathogenesis of muscular dystrophy. Subcell. Biochem. 2007; 45:429–464. [PubMed: 18193647]
11. Millay DP, Goonasekera SA, Sargent MA, Aronow BJ, Molkentin JD. Calcium influx is sufficient to induce muscular dystrophy through a TRPC-dependent mechanism. Proc. Natl. Acad. Sci. U.S.A. 2009; 106:19023–19028. [PubMed: 19864620]
12. Alderton JM, Steinhard RA. How calcium influx through calcium leak channels is responsible for the elevated levels of calcium-dependent proteolysis in dystrophic myotubes. Trends Cardiovasc. Med. 2000; 10:268–272. [PubMed: 11282306]
13. Ruegg U, Nicolas-Métral V, Challet C, et al. Pharmalogical control of cellular calcium handling in dystrophic skeletal muscle. Neuromuscul. Disord. 2002; 12:S155–S161. [PubMed: 12206810]
14. Reed A, Kohl P, Peyronnet R. Molecular candidates for cardiac stretch-activated ion channels. Global Cardiol. Sci. Pract. 2014; 2:9–25.
15. Franco-Obregón A, Lansman JB. Changes in mechanosensitive channel gating following mechanical stimulation in skeletal muscle myotubes from the *mdx* mouse. J. Physiol. 2002; 539:391–407. [PubMed: 11882673]
16. Yeung EW, Whitehead NP, Suchyna TM, Gottlib PA, Sachs F, Allen DG. Effects of stretch-activated channel blockers on $[Ca^{2+}]_i$ and muscle damage in the *mdx* mouse. J. Physiol. 2005; 562:367–380. [PubMed: 15528244]
17. Williams IA, Allen DG. The role of reactive oxygen species in the hearts of dystrophin-deficient mdx mice. Am. J. Physiol. Heart Circ. Physiol. 2007; 293:H1969–H1977. [PubMed: 17573457]
18. Huang H, Wang W, Liu P, et al. TRPC1 expression and distribution in rat hearts. Eur. J. Histochem. 2009; 53:e26. [PubMed: 22073358]
19. Kohl P, Ravens U. Cardiac mechano-electric feedback: past, present, and prospect. Prog. Biophys. Mol. Biol. 2003; 82:3–9. [PubMed: 12732264]
20. Katanosaka Y, Iwasaki K, Ujihara Y, et al. TRPV2 is critical for the maintenance of cardiac structure and function in mice. Nat. Commun. 2014; 5:1–14.
21. Colbert HA, Smith TL, Bargmann CL. OSM-9, a novel protein with structural similiraty to channels, is required for olfaction, mechanosensation, and olfactory adaptation in *Caenorhabditis elegans*. J. Neurosci. 1997; 17:8259–8269. [PubMed: 9334401]
22. Walker RG, Willingham AT, Zuker CS. A Drosophila mechanosensory transduction channel. Science. 2000; 287:2229–2234. [PubMed: 10744543]
23. Patel A, Sharif-Naeini R, Folgering J, Bichet D, Duprat F, Honore E. Canonical TRP channels and mechanotransduction: from physiology to disease states. Pflugers Arch. 2010; 460:571–581. [PubMed: 20490539]
24. Watanabe H, Murakami M, Ohba T, Ono K, Ito H. The pathological role of transient receptor potential channels in heart disease. Circulation. 2009; 73:419–427.
25. Eder P, Molkentin JD. TRPC channels as effector of cardiac hypertrophy. Circ. Res. 2011; 108:265–272. [PubMed: 21252153]
26. Minke B, Cook JA. TRP channel proteins and signal transduction. Physiol. Rev. 2002; 82:429–472. [PubMed: 11917094]
27. Nilius B. From TRPs to SOCs, CCEs, and CRACs: consensus and controversies. Cell Calcium. 2003; 33:293–298. [PubMed: 12765675]
28. Kwan HY, Huang Y, Yao X. Regulation of canonical transient receptor potential isoform 3 (TRPC3) channel by protein kinase G. Proc. Natl. Acad. Sci. U.S.A. 2004; 101:2625–2630. [PubMed: 14983059]

29. Vandebrouck C, Martin D, Colson-Van Schoor M, Debaix H, Gailly P. Involvement of TRPC in the abnormal calcium influx observed in dystrophic (*mdx*) mouse skeletal muscle fibers. J. Cell Biol. 2002; 158:1089–1096. [PubMed: 12235126]
30. Ward ML, Williams IA, Chu Y, Cooper PJ, Ju YK, Allen DG. Stretch-activated channels in the heart: contributions to length-dependence and to cardiomyopathy. Prog. Biophys. Mol. Biol. 2008; 97:232–249. [PubMed: 18367238]
31. Sabourin J, Lamiche C, Vandebrouck A, Magaud C, Rivet J, Cognard C, Bourmeyster N, Constantin B. Regulation of TRPC1 and TRPC4 cation channels requires an alpha1-syntrophin-dependent complex in skeletal mouse myotubes. J. Biol. Chem. 2009; 284:36248–36261. [PubMed: 19812031]
32. Zhao X, Moloughney JG, Zhang S, Komazaki S, Weisleder N. Orai1 mediates exacerbated Ca($^{2+}$) entry in dystrophic skeletal muscle. PLoS ONE. 2012; 7(11):e49862. [PubMed: 23185465]
33. Maroto R, Raso A, Wood TG, Kurosky A, Martinac B, Hamill OP. TRPC1 forms the stretch-activated cation channel in vertebrate cells. Nat. Cell Biol. 2005; 7:179–185. [PubMed: 15665854]
34. Bowman CL, Gottlib PA, Suchyna TM, Murphy YK, Sachs F. Mechanosensitive ion channels and the peptide inhibitor GsMTx-4: history, properties, mechanisms and pharmacology. Toxicon. 2007; 49:249–270. [PubMed: 17157345]
35. Spassova MA, Hewavitharana T, Xu W, boloff J, Gill DL. A common mechanism underlies stretch activation and receptor activation of TRPC6 channels. Proc. Natl. Acad. Sci. U.S.A. 2006; 103:16586–16591. [PubMed: 17056714]
36. Riccio A, Medhurst AD, Mattei C, et al. mRNA distribution analysis of human TRPC family in CNS and peripheral tissues. Brain Res. 2002; 109:95–104.
37. Dyachenko V, Husse B, Rueckschloss U, Isenberg G. Mechanical deformation of ventricular myocytes modulates both TRPC6 and Kir2.3 channels. Cell Calcium. 2009; 45:38–54. [PubMed: 18635261]
38. Dyachenko, V.; Isenberg, G. Ventricular myocytes: deformation induced sarcomere misalignment modulates TRPC6 and KIR2.3 channels. Proceedings of the Fourth International Conference on Cardiac Mechano-Electric Feedback; 2007. p. P.84
39. Muraki K, Iwata Y, Katanosaka Y, et al. TRPV2 is a component of osmotically sensitive cation channels in murine aortic myocytes. Circ. Res. 2003; 93:829–838. [PubMed: 14512441]
40. Iwata Y, Ohtake H, Suzuki O, Matsuda J, Komamura K, Wakabayashi S. Blockade of sarcolemmal TRPV2 accumulation inhibits progression of dilated cardiomyopathy. Cardiovasc. Res. 2013; 99:760–768. [PubMed: 23786999]
41. Lorin C, Vögeli I, Niggli E. Dystrophic cardiomyopathy—role of TRPV2 channels in stretch-induced cell damage. Cardiovasc. Res. 2015; 106:153–162. [PubMed: 25616416]
42. Rubinstein J, Lasko VM, Koch SE, et al. Novel role of transient receptor potential vanilloid 2 in the regulation of cardiac performance. Am. J. Physiol. Heart Circ. Physiol. 2014; 306:H574–H584. [PubMed: 24322617]
43. Iwata Y, Arai Y, Komamura K, Miyatake K, Shinohara M. A novel mechanism of myocyte degeneration involving the Ca^{2+}-permeable growth factor-regulated channel. J. Cell Biol. 2003; 131:957–967. [PubMed: 12796481]
44. Harisseh R, Chatelier A, Magaud C, Déliot N, Constantin B. Involvement of TRPV2 and SOCE in calcium influx disorder in DMD primary human myotubes with a specific contribution of α1-syntrophin and PLC/PKC in SOCE regulation. Am. J. Physiol.—Cell Physiol. 2013; 304:C881–C894. [PubMed: 23426965]
45. Fabiato A. Myoplasmic free calcium concentration reached during the twitch of an intact isolated cardiac cell and during calcium-induced release of calcium from the sarcoplasmic reticulum of a skinned cardiac cell from the adult rat or rabbit ventricle. J. Gen. Physiol. 1981; 78:457–497. [PubMed: 6796647]
46. Brady AJ. Mechanical properties of isolated cardiac myocytes. Physiol. Rev. 1991; 71:413–428. [PubMed: 2006219]
47. Prosser BL, Ward CW, Lederer JW. X-ROS signaling: rapid mechano-chemo transduction in heart. Science. 2011; 333:1440–1445. [PubMed: 21903813]

48. Fanchaouy M, Polakova E, Jung C, Ogrodnik J, Shirokova N, Niggly E. Pathways of abnormal stress-induced Ca^{2+} influx into dystrophic mdx cardiomyocytes. Cell Calcium. 2009; 46:114–121. [PubMed: 19604578]
49. Isenberg, G.; Kondratev, D.; Dyachenko, V.; Kazanski, V.; Gallitelli, MF. Mechanosensitivity in Cells and Tissues. Academia; Moscow: 2005. Isolated cardiomyocytes: mechanosensitivity of action potential, membrane current and ion concentration.
50. Le Guennec JY, Peineau N, Arbigay J, Mongo KG, Garnier D. A new method of attachment of isolated mammalian ventricular myocytes for tension recording: length dependence of passive and active tension. J. Mol. Cell. Cardiol. 1990; 22:1083–1093. [PubMed: 2095433]
51. Sugiera S, Nishimura S, Yasuda S, Hosoya Y, Katoh K. Carbon fiber technique for the investigation of single-cell mechanics in intact cardiac myocytes. Nat. Protoc. 2006; 1:1453–1457. [PubMed: 17406434]
52. Yasuda SI, Sugiura S, Kobayawa N, et al. A novel method to study contraction characteristics of a single cardiac myocyte using carbon fibers. Am. J. Physiol. Heart Circ. Physiol. 2001; 281:H1442–H1446. [PubMed: 11514317]
53. Kabaeva Z, Zhao M, Michele DE. Blebbistatin extends culture life of adult mouse cardiac myocytes and allows efficient and stable transgene expression. Am. J. Physiol. Heart Circ. Physiol. 2008; 294:H1667–H1674. [PubMed: 18296569]
54. Tutdibi O, Brinkmeier H, Rüdel H, Föhr KJ. Increased calcium entry into dystrophin-deficient muscle fibres of MDX and ADR-MDX mice is reduced by ion channel blockers. J. Physiol. 1999; 515:859–868. [PubMed: 10066910]
55. Iwata Y, Katanosaka Y, Arai Y, Shigekawa M, Wakabayashi S. Dominant negative inhibition of calcium influx via TRPV2 ameliorates muscular dystrophy in animal models. Hum. Mol. Genet. 2009; 18:824–834. [PubMed: 19050039]
56. Neeper MP, Liu Y, Hutchinson TL, Wang Y, Flores CM, Qin N. Activation properties of heterologously expressed mammalian TRPV2: evidence for species dependence. J. Biol. Chem. 2007; 282:15894–15902. [PubMed: 17395593]
57. Hopf FW, Reddy P, Hong J, Steinhardt RA. A capacitative calcium current in cultured skeletal muscle cells is mediated by the calcium-specific leak channel and inhibited by dihydropyridine compounds. J. Biol. Chem. 1996; 271:22358–22367. [PubMed: 8798397]
58. Vandebrouck A, Sabourin J, Rivet J, Balghi H, Sebille S, Kitzis A, Raymond G, Cognard C, Bourmeyster N, Constantin B. Regulation of capacitative calcium entries by alpha1-syntrophin: association of TRPC1 with dystrophin complex and the PDZ domain of alpha1-syntrophin. FASEB J. 2007; 21:608–617. [PubMed: 17202249]
59. He LP, Hewavitharana T, Soboloff J, Spassova MA, Gill DL. A functional link between store-operated and TRPC channels revealed by the 3, 5-bis(trifluoromethyl)pyrazole derivative, BTP2. J. Biol. Chem. 2005; 280:10997–11006. [PubMed: 15647288]
60. Ishikawa J, Ohga K, Yoshino T, Takezawa R, Ichikawa A, Kubota H, Yamada T. A pyrazole derivative YM-58483, potently inhibits store-operated sustained Ca^{2+} influx and IL-2 production in T lymphocytes. J. Immunol. 2003; 1:4441–4449. [PubMed: 12707319]
61. Suchyna TM, Johnson JH, Hamer K, et al. Identification of a peptide toxin from *Grammostola spatulata* spider venom that blocks cation-selective stretch-activated channels. J. Gen. Physiol. 2000; 115:583–598. [PubMed: 10779316]
62. Gottlieb P, Folgering J, Maroto R, et al. Revisiting TRPC1 and TRPC6 mechanosensitivity. Pflugers Arch. 2007; 455:1097–1103. [PubMed: 17957383]
63. Iwata Y, Katanosaka Y, Arai Y, Shigekawa M, Wakabayashi S. Dominant negative inhibition of calcium influx via TRPV2 ameliorates muscular dystrophy in animal models. Hum. Mol. Genet. 2009; 18:824–834. [PubMed: 19050039]
64. Stiber J, Hawkins A, Zhang ZS, Wang S, Burch J, Graham V, Ward CC, Seth M, Finch E, Malouf N, Williams RS, Eu JP, Rosenberg P. STIM1 signaling controls store-operated calcium entry required for development and contractile function in skeletal muscle. Nat. Cell Biol. 2008; 10:688–697. [PubMed: 18488020]
65. Suchyna TM, Sachs F. Mechanosensitive channel properties and membrane mechanics in mouse dystrophic myotubes. J. Physiol. 2007; 581:369–387. [PubMed: 17255168]

66. Hino N, Ochi R, Yanagisawa T. Inhibition of the slow inward current and the time-dependant outward current of mammalian ventricular muscle by gentamicin. Pflugers Arch. 1982; 394:243–249. [PubMed: 7145605]

67. Belus A, White E. Effects of streptomycin sulfate on I(CaL) I(Kr) and I(Ks) in guinea-pig ventricular myocytes. Eur. J. Pharmacol. 2002; 445:171–178. [PubMed: 12079681]

68. Kamkin A, Kiseleva I, Isenberg G. Ion selectivity of stretch-activated cation currents in mouse ventricular myocytes. Pflügers Arch. 2003; 446:220–231. [PubMed: 12739160]

69. Naeini RS, Witty M-F, Séguéla P, Bourque CW. An N-terminal variant of Trpv1 channel is required for osmosensory transduction. Nat. Neurosci. 2006; 9:93–98. [PubMed: 16327782]

70. Caprodossi S, Lucciarini R, Amantini C, Nabissi M, Canesin G, Ballarini P, Di Spilimbergo A, Cardarelli MA, Servi L, Mammana G, Santoni G. Transient receptor potential vanilloid type 2 (TRPV2) expression in normal urothelium and in urothelial carcinoma of human bladder: correlation with the pathologic stage. Eur. Urol. 2008; 54:612–620. [PubMed: 17977643]

71. Thalmann GN. Prognostic markers for bladder cancer—are we there yet? Eur. Urol. 2007; 51:591–592. [PubMed: 17174022]

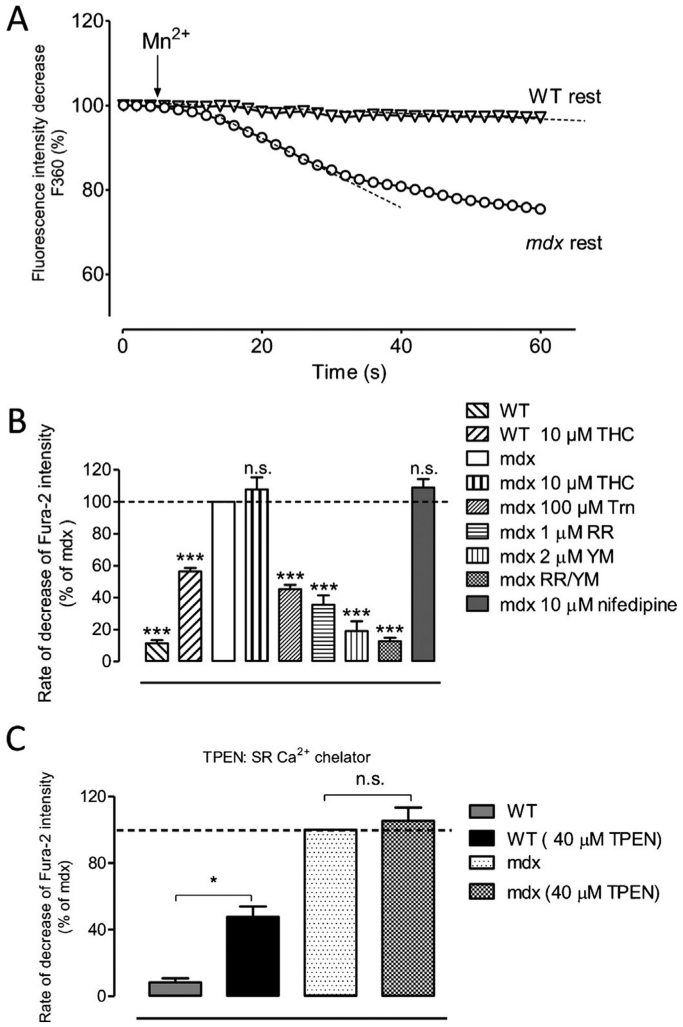

Fig. 1. Cation influx in resting isolated cardiomyocytes, quenching of fura-2 with the manganese quench technique

(A) Representative recordings of fura-2 fluorescence during superfusion with a calcium-free Tyrode solution containing 300 µM Mn^{2+}, obtained in resting WT (open triangles) and *mdx* (open circles) cardiomyocytes. (B) Mn^{2+} influx in isolated WT in the presence of SACs and SOCs activators and inhibitors. WT cells were incubated with 10 µM THC for TRPV2 activation; *mdx* cardiomyocytes were incubated in the presence of 10 µM THC, 100 µM Tranilast (Trn) and 1 µM Ruthenium Red (RR) for TRP inhibition, 2 µM YM-58483 (YM), the combination of 1 µM RR and 2 µM YM and 10 µM Nifedipine. Measurements are represented as rate of decrease of fura-2 intensity, relative to the rate measured in mdx cardiomyocytes (100%, open bar). Rates of decrease in % of the mean control value in mdx ($n = 6$) taken as 100: WT: 11.5 ± 2.6 $n = 4$; WT 10 µM THC: 56.4 ± 3.8 $n = 6$; mdx 10 µM THC: 107.8 ± 19.9 $n = 7$; mdx 100 µM Trn: 45.4 ± 8.3 $n = 10$; mdx 1 µM RR: 35.6 ± 5.8 $n = 8$; mdx 2 µM YM: 19.2 ± 6.1 $n = 9$; mdx RR/YM: 12.7 ± 2.1 $n = 6$; mdx 10 µM nifedipine: 109 ± 5.1 $n = 9$. (C) Mn^{2+} influx in WT and mdx cardiomyocytes in the presence of 40 µM of the SR Ca^{2+} chelator TPEN. WT cells were incubated with 10 µM THC for TRPV2 activation. Rates of decrease in % of the mean control value in mdx ($n = 7$) taken as 100:

WT: 8.5 ± 2.4 $n = 4$; WT 40 μM TPEN: 47.7 ± 6.3 $n = 6$; mdx 40 μM TPEN: 105.4 ± 7.9 $n = 7$. *** $P < 0.001$; * $P < 0.5$; ns, not significant.

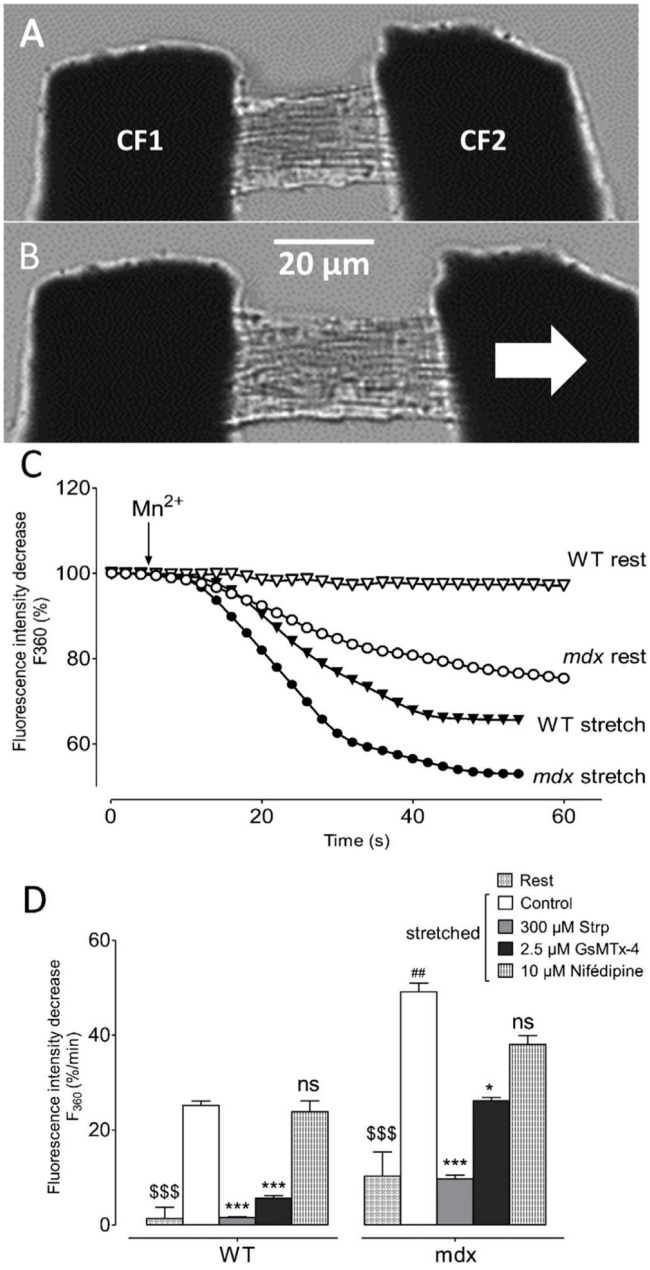

Fig. 2. Stretch-dependent calcium entry in WT and mdx cardiomyocytes

(A and B) Images of an isolated cardiomyocyte attached to two carbon fibres (CF) and stretched. The two fibres were connected to micromanipulators (3 axis) allowing to gently move each fibre. In this protocol, the fibre on left (CF1 in A) served as an anchor with no movement during the experiment time. Axial stretch was carried out through lateral movement of the fibre on right (CF2 in A and the bold white arrow in B). Axial stretch was applied for 30 s before Mn^{2+} application and was maintained during the recording time, i.e. around 60 s. (C) Representative recordings of fura-2 fluorescence during perfusion with 300 µM Mn^{2+} obtained in resting WT (open triangles) and *mdx* (open circles) cardiomyocytes and in stretched WT (black triangles) and *mdx* (black circles). D: quenching rate in the

presence of SACs inhibitors in axial-stretched WT and *mdx* cardiomyocytes. Cells were incubated with 300 μM streptomycin (Strp, grey bars) or 2.5 μM GsMTx-4 (Black bars) for SACs inhibition and with 10 μM nifedipine (vertical hatching). Open bars represent the quenching rate in stretch control conditions and declined hatching bars report manganese quenching rate in resting conditions. Measurements are represented as slopes of the Mn^{2+}-induced decreasing phase of fura-2 and expressed as percent per minute. Bar graphs represent mean rates of fluorescence decrease induced by Mn^{2+} ± SEM. * $P < 0.01$; *** $P < 0.001$; ns, not significant. $^{\#\#}$Represents the statistical difference between WT and *mdx* in stretch conditions. $^{\#\#}$ $P < 0.005$; $^{\$\$\$}$ represents the statistical difference between resting and stretch conditions. $^{\$\$\$}$ $P < 0.001$.

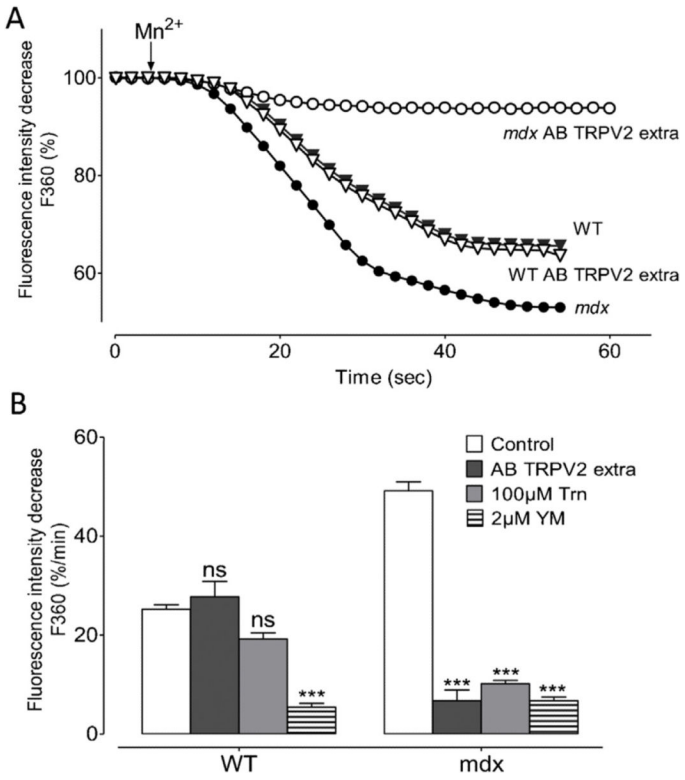

Fig. 3. Influx in stretched cardiomyocytes in presence of TRPV2 channels antibodies

(A) example of recordings of fura-2 fluorescence during perfusion with 300 µM Mn^{2+} obtained from stretched WT (black triangles) and stretched *mdx* (black circles) and after incubation with antibody against TRPV2 (AB TRPV2 extra) from stretched WT (open triangles) and *mdx* (open circles) cardiomyocytes. (B) Effect of inhibitors on manganese quench rate in stretched cardiomyocytes. Stretched cells were pre-incubated with antibody against an extracellular epitope of TRPV2 (dark grey bars), 100 µM tranilast (clear grey bars) and 2 µM YM-48483 (horizontal hatching bars) in stretched WT and mdx cardiomyocytes. Open bars represent the control. Measurements are represented as slopes of the Mn^{2+}-induced decreasing phase of fura-2 fluorescence and expressed as percent of decrease per minute. Bar graphs represent maximal rates of fluorescence decrease induced by Mn^{2+} ± SEM. *** $P < 0.001$; ns, not significant.

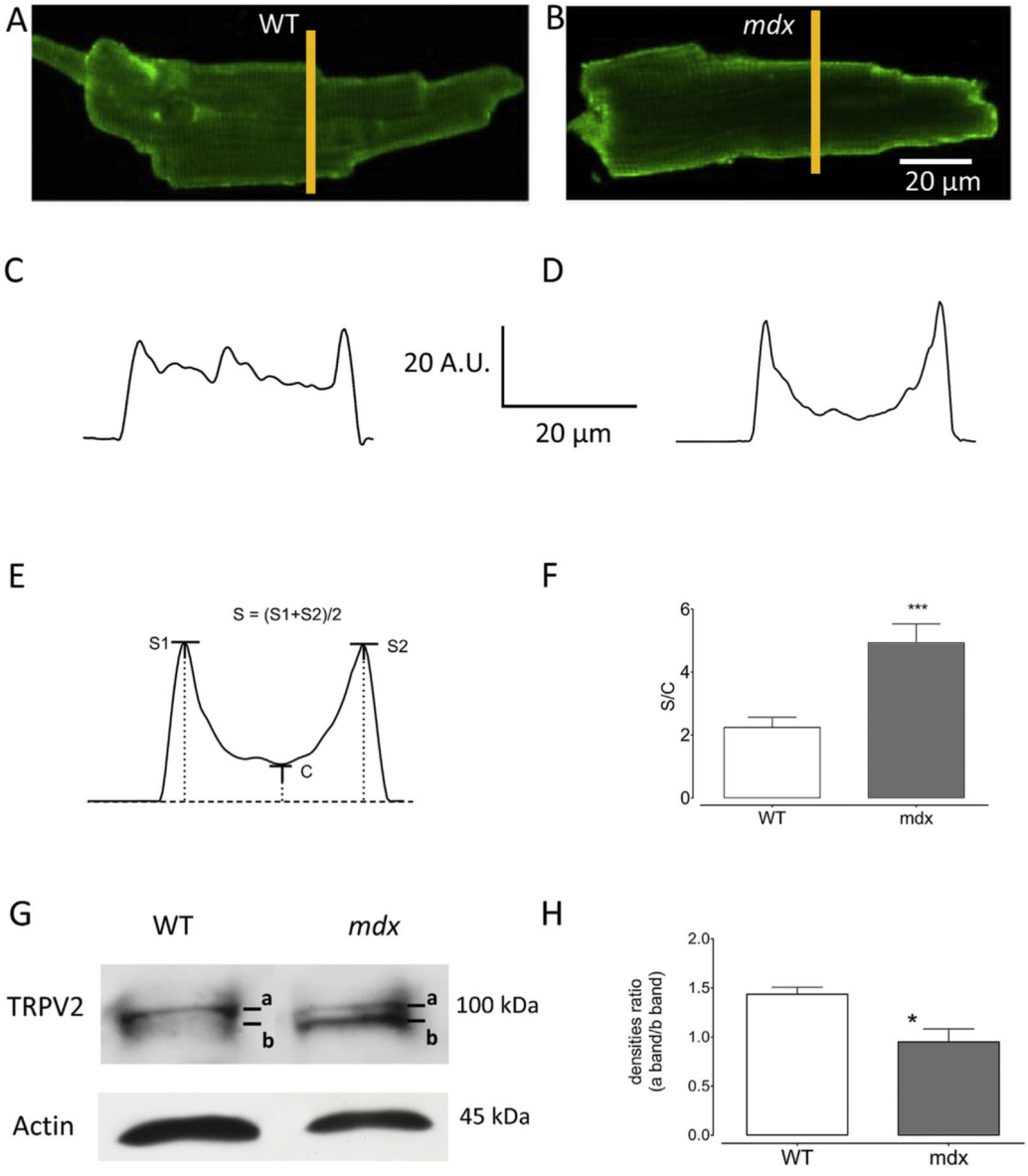

Fig. 4. TRPV2 protein expression in isolated WT and mdx cardiomyocytes

(A and B) Examples of immunostaining images of TRPV2 channels in WT and *mdx* cardiomyocytes, respectively. In each image, the drawn vertical yellow line represents the area selected for plotting a fluorescence profile. (C) Fluorescence amplitude profile from WT in (A). (D) Fluorescence amplitude profile from *mdx* in (B). From several images, quantification of the fluorescence intensity at the periphery of the cell, relative to intracellular fluorescence intensity, has been performed (E and F). From profiles, we determined the sarcolemmal fluorescence intensities S1 and S2 (panel E) and the mean (S) of these two values was divided by the minimal fluorescence intensity value (level C in the panel E) found in the profile of panel (E). The determined ratio S/C was calculated from images in WT (n = 11 cells) and *mdx* (n = 13 cells) cardiomyocytes. (G) Example of western blot obtained from isolated ventricular WT and *mdx* cardiomyocytes. A two bands (*a* and *b*) profile was observed with a marked presence of a light band in *mdx* sample. (H)

The proportion of the two bands was evaluated through the calculation of the ratio of the band densities (*a* band density/*b* band density). *** $P < 0.001$, * $P < 0.01$.

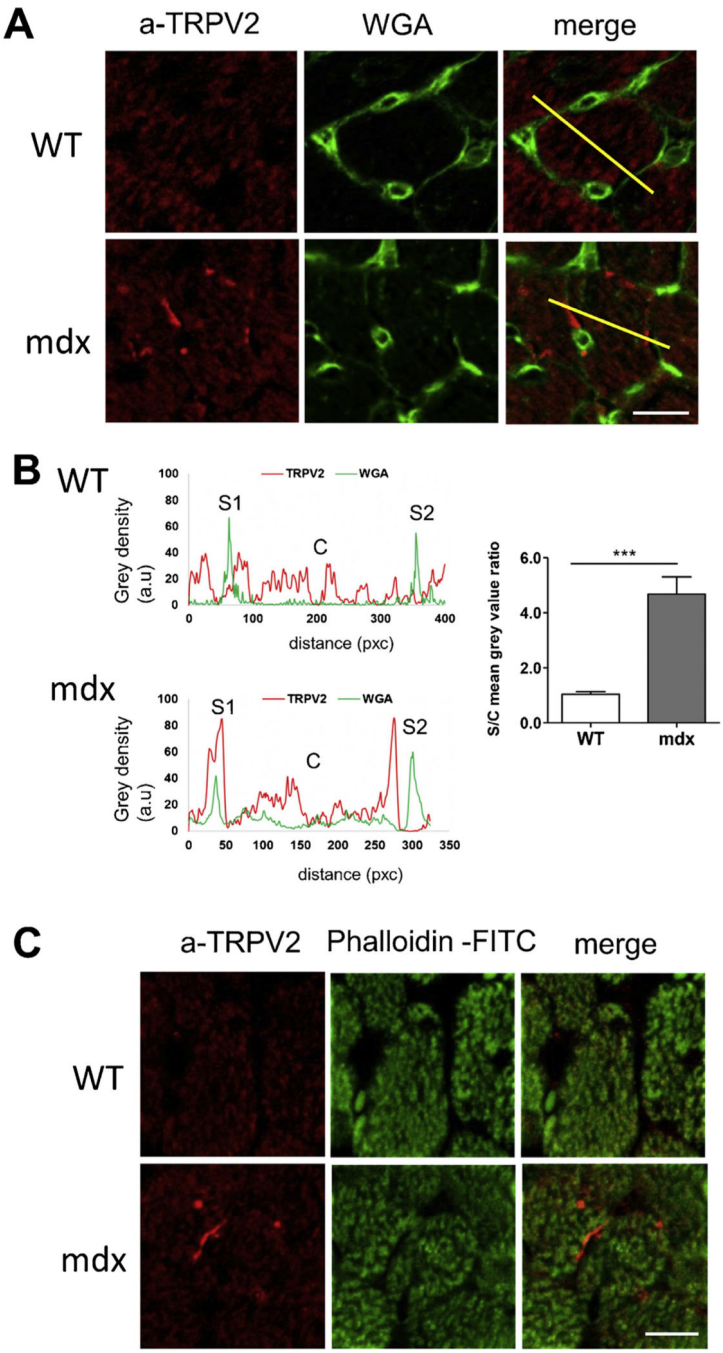

Fig. 5. TRPV2 expression in heart tissue from WT and mdx mice

Immunolocalization of TRPV2 channels (red) within cardiomyocytes (transversal sections from left ventricle). Confocal immunofluorescence. (A) Green—sarcolemma and capillary position (WGA staining). The drawn yellow line represents an area selected for plotting a fluorescence profile. (B) Left panel: Profiles showing the optical density (grey plot) along the yellow line (in A). Red—TRPV2 profile; green—WGA staining profile. The WGA fluorescence intensities at S1 and S2 correspond to the sarcolemma position; the WGA fluorescence intensities at C corresponded to the cytosol position. The quantification of the

TRPV2 (red) fluorescence intensity was performed at the periphery of the cell (sarcolemma position) and at the central position (cytosol). Right panel. The determined ratio S/C calculated from images in WT (n = 8 cells) and mdx (n = 8 cells) cardiomyocytes showing accumulation of TRPV2 in the sarcolemma of mdx mice. (C) Green—sarcomere position (F-actin, phalloidin staining). Typical representative image from 3 WT and 3 mdx mice. Bar −10 μm. *** $P < 0.001$.